



Biocompatible silk fibroin scaffold prepared by reactive inkjet printing

Patrick Rider¹, Yu Zhang², Christopher Tse³, Yi Zhang³, Dharana Jayawardane², Jonathan Stringer³, Jill Callaghan¹, I. M. Brook¹, Cheryl A. Miller^{1,*}, Xiubo Zhao², and Patrick J. Smith³

¹ School of Clinical Dentistry, The University of Sheffield, Sheffield S10 2TA, UK

² Department of Chemical and Biological Engineering, The University of Sheffield, Sheffield S1 3JD, UK

³ Department of Mechanical Engineering, The University of Sheffield, Sheffield S1 3JD, UK

Received: 29 March 2016

Accepted: 4 June 2016

Published online:
16 June 2016

© The Author(s) 2016. This article is published with open access at Springerlink.com

ABSTRACT

It has recently been shown that regenerated silk fibroin (RSF) aqueous solution can be printed using an inkjet printer. In this communication, we demonstrate an alternative reactive inkjet printing method that provides control over RSF crystallinity through β -sheet concentration. A biocompatible film has successfully been produced through the alternate printing of RSF aqueous solution and methanol using reactive inkjet printing. Control over the formation of the β -sheet structure was achieved by printing different ratios of RSF to methanol and was confirmed using Fourier Transform Infra Red spectroscopy. The biocompatibility of the printed silk scaffold was demonstrated by the growth of fibroblast cells upon its surface.

Silk is a versatile, natural material favoured for its mechanical strength, excellent biocompatibility, adaptable biodegradability [1, 2], easy processing [3] and flexible structural modification [4]. Silk has a long history of use [5]; recently, regenerated silk fibroin (RSF) has been used as a building block for the fabrication of biomedical devices [3]. RSF structures are commonly produced with a casting method; however, additive manufacture applications offer a greater control over RSF film surfaces which can be advantageous for controlling cell growth. Current additive manufacture applications are mainly focused on producing individual silk fibres such as electrohydrodynamic printing [6] and electrospinning [7].

Different silk polymorphs, silk I, silk II and silk III, have been observed. Silk I, which is the water-soluble state seen prior to crystallisation, is composed of α -helix and amorphous chains. Silk II contains an extended β -sheet structure and appears after spinning [3]. Silk III assembles at an air (or oil)/water interface [8], but only silk I and silk II are of interest in this work. Water-soluble silk I can be converted to insoluble silk II by exposure to methanol, as reported by Huemmerich et al. [9]. The asymmetrical β -sheet structures of Silk II consist of hydrogen side chains from glycine on one side and methyl side chains from alanine on the other side. The methyl groups interact with hydrogen groups of opposing β -sheets to form

Address correspondence to E-mail: c.a.miller@sheffield.ac.uk

the inter-sheet stacking during crystallisation. Strong hydrogen bonds and van der Waals forces generate a thermodynamically stable structure.

The structure transition of RSF is an important property that has been utilised for the fabrication of thin films, electrospun fibres, hydrogels and 3D porous scaffolds [3]. By increasing the β -sheet content using approaches such as controlled drying and alcohol immersion, the mechanical properties of RSF films can be improved. Similarly, the degradation rate of RSF can be controlled by varying the processing route [1, 2]. For instance, water-annealed films are more flexible and have a faster degradation rate than that of methanol treated films [1]. Silk degrades into non-harmful peptides and free amino acids that can be easily removed by the body [10], which is superior to materials such as polyesters that degrade into acidic by-products, leading to increased levels of inflammation around the implant site. All these properties (two polymorphs with different solubility, controllable crystal structure and degradation) make RSF a promising candidate for biomaterial fabrication, and in particular, an excellent bio-ink for inkjet printing.

As a versatile manufacturing method, inkjet printing is used in applications as diverse as organic electronics [11], ceramics [12], tissue engineering [13] and protein-based diagnostics [14]. Inkjet was recognised as a means for controlling reactions over 20 years ago [15]. The proportions of reactants can be readily controlled due to the high degree of reproducibility in the size, number and placement of droplets on to a substrate. Inkjet printing builds structures layer by layer, which gives greater control over the finished product and, if required allows a substrate to be selectively patterned. The inkjet printing of silk materials is becoming a topic of interest as demonstrated by Suntivich et al. who modified silk side chains with poly-(L-lysine) and poly-(L-glutamic acid) to produce oppositely charged polyelectrolytes which were then inkjet printed and paired in bilayers to produce a silk II structure. By building up layers of bilayers, silk nests were produced which were used for cell entrapment [16]. Tao et al. has recently communicated the inkjet printing of 2D patterns using functional silk inks blended with different active components such as gold nanoparticles, enzymes and antibiotics [17]. In this communication, we use reactive inkjet printing as an alternative approach to synthesise silk II alongside

selective patterning. Two inks are used, one is aqueous silk I and the second is methanol, which allows us to control silk polymorph concentrations in situ, thus controlling mechanical properties. This is contrary to the work of Tao et al. who used a single ink approach; they postulated that a biomaterial composite ink needs to be formulated in order to control mechanical properties.

For this investigation, RSF was obtained following Ajisawa's method [18]. Briefly, native silk was degummed by boiling in 0.02 M sodium carbonate (Na_2CO_3). The degummed silks were rinsed with distilled water three times until they looked visibly clear before being dried in an oven at 30 °C overnight. 1.5 g of the degummed fibroin was added to 10 g of Ajisawa's reagent (a reagent mixed of CaCl_2 /ethanol/water with a 1:2:8 respective molar ratios). The mixture was stirred at 75 °C for 3 h and left to cool. The solution was dialysed in distilled water to remove the salts. Next, the dialysed RSF solution was centrifuged at 10000 rpm for 15 min before being filtered to a purer solution. Gel electrophoresis was performed and indicated that the heavy chain of fibroin degraded to give molecular weights in the range of 25–370 kDa. Three concentrations were prepared: 5, 10 and 100 mg mL^{-1} .

A Jetlab 4 (MicroFab, Plano, TX) fitted with 60 μm piezo printheads was used for the printing of RSF. The printing parameters used for the two inks (RSF and methanol) were 70–95 V and frequencies ranged from 150 to 300 Hz.

To demonstrate that RSF can be used to fabricate 3D structures, pillared structures were produced by printing a 5-by-5 dot array with a spacing of 0.5 mm. A singular layer of RSF ink was printed followed by a layer of printed methanol. Printing was paused for 10 s to allow for solvent evaporation before subsequent layers were printed. Structures of different heights were achieved by printing 200, 300, 400, 600, 800 and 1000 layers using RSF ink with concentrations of 5 and 10 mg mL^{-1} .

Scanning electron microscopy (SEM) (Camscan Mk 2) was used to examine the surface structure of the printed samples with 300 layers. The SEM showed an ordered array of 200 μm diameter pillars, demonstrating the printability and precise control obtained by inkjet printing (Fig. 1a). Interferometry (Contour GT 3D Optical Microscope) was used to obtain the precise height and 3D morphology of the pillars. For each sample, five randomly selected pillars were

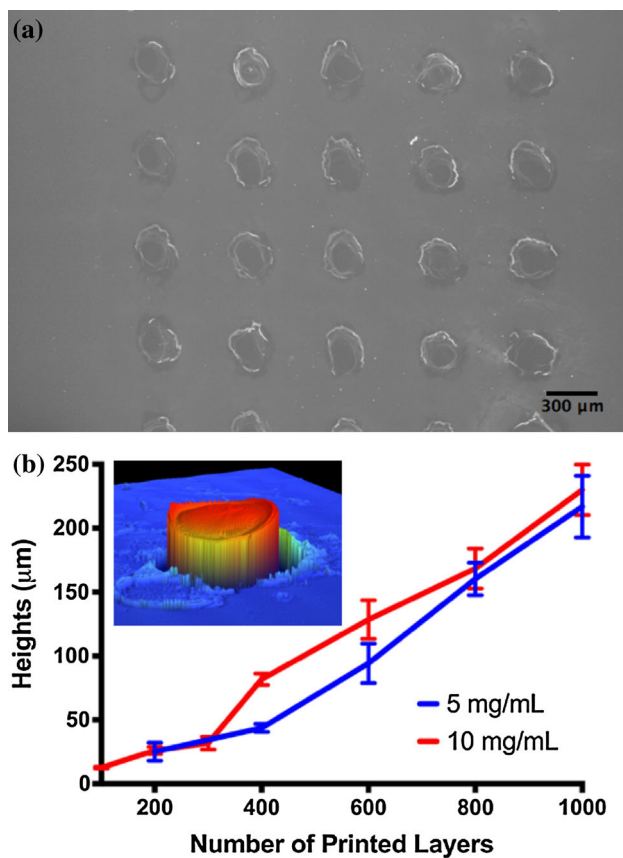


Figure 1 a SEM of 5-by-5 array printed up to 300 layers with a RSF concentration of 10 mg mL^{-1} . b Relationship between height and number of RSF layers printed with concentrations of 5 and 10 mg mL^{-1} . The inset is an interferometry image of a pillar after 100 layers.

measured. Increasing the number of layers deposited steadily raised the average height of the silk structures. The concentration of the ink was not critical for determining the height of the pillars. As only height has been measured and not the width of the pillar's base, it is possible that the profile of the pillars produced with the 10 mg mL^{-1} concentration is greater than that of the lower 5 mg mL^{-1} concentration, similar to the behaviour reported by van den Berg et al. [19]. Variation in pillar height could have been caused by the settlement of material [19]. Heights of pillars with equal layers remained relatively constant up to 800 printed layers and a height of $160 \mu\text{m}$ (Fig. 1b).

The droplet volume, estimated to be 113 pL , along with height and number of droplets per pillar enabled pillar densities to be calculated. The density of bulk silk is 1250 kg m^{-3} . Dividing the density of each pillar by the density of bulk silk gives the

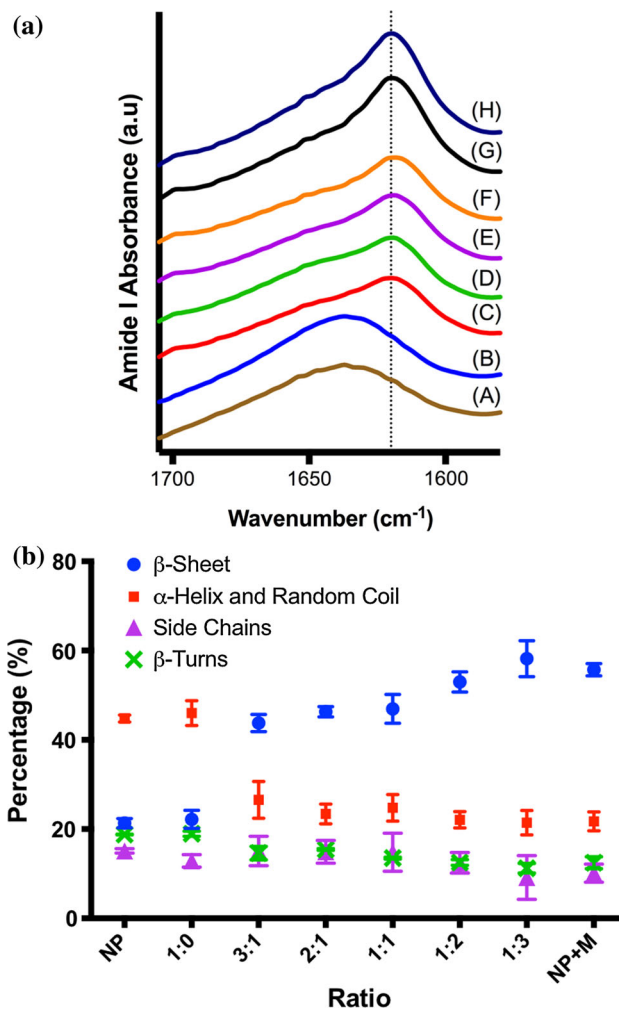


Figure 2 a FTIR spectra of the amide I region of printed silk films with printed volume ratios (B) 1:0 (C) 3:1 (D) 2:1 (E) 1:1 (F) 1:2 and (G) 1:3 of silk (100 mg mL^{-1}) to methanol. Non-printed cast films (NP) and cast films with methanol treatment (NP+M) are shown with lines (A) and (H), respectively. The vertical dashed line represents the band at 1620 cm^{-1} , indicative of β -sheets. b Percentage of component secondary structures for each of the printed silk film ratios; β -sheets (circles), α -helix and random coils (squares), turns (crosses) and side chains (triangles).

percentage fraction of silk and hence a measure of pillar porosity. The average porosities produced for the 5 and 10 mg mL^{-1} were around 90 %.

Silk films were then produced by printing layers of overlapping droplets on top of glass cover slips using the same procedure as described above. Twenty layers of RSF were printed to produce a regenerated silk film. Fourier Transform Infrared (FTIR) Spectroscopy (PerkinElmer Spectrum 2000) measured in attenuated total reflection were taken on samples

which had been prepared by printing with alternating layers of RSF and methanol, where RSF was printed at a concentration of 100 mg mL^{-1} . RSF:methanol volume ratios were 1:0, 3:1, 2:1, 1:1, 1:2 and 3:1. Non-printed cast RSF films (NP) and cast films submerged in methanol for 4 days (NP+M) to induce β -sheet formation were used as controls to monitor the transformation of the printed films. FTIR spectra were taken of the amide I region ($1705\text{--}1595 \text{ cm}^{-1}$), which is most commonly used to determine the secondary structure of proteins as this region has less convolution of peaks than other areas of the spectra [2, 20]. Films untreated with methanol had a peak at 1638 cm^{-1} , associated with random coils; however, with the increasing volumes of methanol, this peak shifts to 1620 cm^{-1} which is indicative of β -sheets [21], and in (Fig. 2a), this peak is marked with a vertical *dashed line*.

Fourier self deconvolution (FSD) of the amide I spectra was performed by OriginPro 2016 software using the technique previously described by Hu et al. [21]. The newly found bands were used to identify different component secondary structures of each of the spectra. Integrated values for each component

were used to calculate the percentage of; β -sheet, α -helix and random coils, turns and side chains present within the different films (Fig. 2b). Error bars were created by performing FSD of the spectra with different half-bandwidths of 15, 20, 25 and 30 cm^{-1} . The percentage of β -sheet significantly increases by 22 % with the addition of methanol when comparing the ratios of 1:0 to 3:1 and remains relatively constant before a significant increase between the ratios 1:2 and 1:3. The controls of NP and NP+M were significantly similar to printed films without methanol treatment (1:0) and films with the highest methanol ratios (1:2 and 1:3), respectively.

To demonstrate the potential of using inkjet to produce gradients or domains of different crystallinity within RSF structures, films of printed RSF were selectively patterned with methanol (Fig. 3a). Lines of methanol were printed upon the RSF films with a ratio of 1:2 RSF (100 mg) to methanol (1 mL). The films were then submerged in water for 3 h, after which the untreated areas of the films had almost completely dissolved leaving only the methanol treated domains (Fig. 3b). The accuracy and flexibility of printed pattern designs was also demonstrated

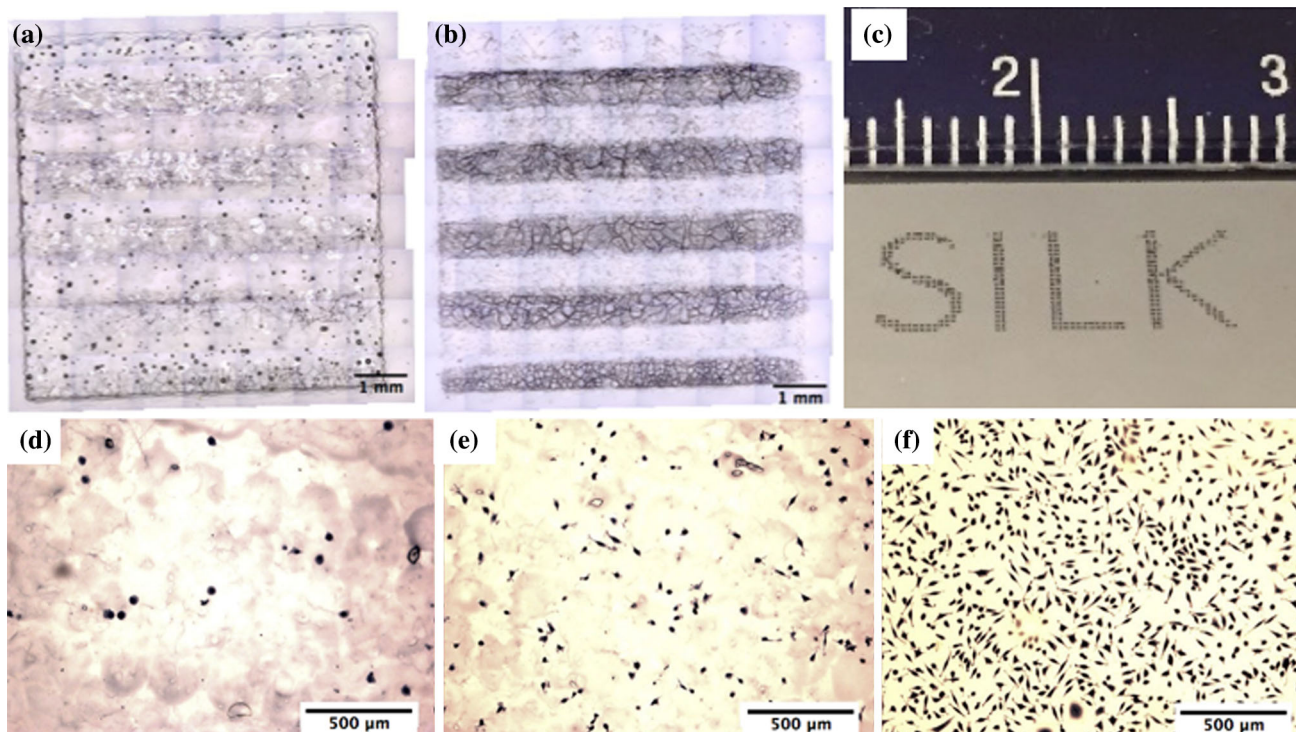


Figure 3 a, b Silk films with selectively printed methanol treated domains. a Silk film after printing. b Silk film after 3 h submerged in water. c ‘SILK’ pattern directly printed using 10 mg mL^{-1} RSF

solution. d, e L929 cells seeded onto regenerated silk films after d 1 day, e 2 days and f 5 days. Cell nucleus and body stained with Haematoxylin, where *scale bar* indicates $500 \mu\text{m}$.

in Fig. 3c. As discussed earlier, the ability to selectively induce regions of different crystallinity could be used to control degradation rate, since the degradation of RSF structures is related to their β -sheet content [1, 2]. Inkjet printing offers greater flexibility in controlling the crystallinity of the RSF structure due to its selectively patterning nature.

Simple cell studies were conducted to evaluate the biocompatibility of printed RSF films. Samples were first sterilised with methanol before being seeded with Murine Fibroblast (L929) cells. After 5 days submerged in media and incubated at 37 °C, all silk films remained on the substrate. This would be expected as the degradation of silk relies on the presence of enzymes to break down its structure.

After a 5-day incubation period, fibroblast cells were seen to produce confluent layers over the RSF film surfaces (Fig. 3d–f). Cellular adhesion and proliferation over the printed RSF film surfaces suggest biocompatibility of films produced via inkjet printing.

In conclusion, RSF structures have been produced using reactive inkjet printing. Specifically, a reactive inkjet printing method for manufacturing RSF constructs with controllable β -sheet content has been described in which water-soluble RSF solution was printed first followed by the printing of methanol which converted silk I into silk II. Stable RSF pillars were successfully printed to a height of 230 μm with a diameter of 200 μm . The printed silk pillars could potentially be employed as scaffolds for tissue engineering [22].

By regulating the amount of methanol printed on top of the deposited RSF, the β -sheet content of the RSF structures could be controlled. As the β -sheet content of silk is related to its degradation rate, inkjet printing can potentially be used to control the degradation rate of the RSF structures. Within tissue engineering applications, adapting the degradation rate of the material to correlate with the regeneration of the surrounding tissue could improve regeneration of a defect site, which makes the process reported in this communication attractive compared to other additive manufacturing processes used to make RSF structures. Finally, the inkjet-printed RSF films have shown to be biocompatible with fibroblast cellular adhesion and proliferation on film surfaces. Overall, inkjet printing has been demonstrated as a method which offers control over surface structure, similar to other additive manufacture processes and more precise than casting methods. It has also shown that with

inkjet printing it is possible to control silk crystallinity with a single-step process.

Acknowledgements

The authors would like to thank EPSRC (EP/N007174/1) and Nobel Biocare UK for their support in funding this research. Miller and Brook are members of the UK EPSRC Centre for Innovative Manufacturing for Medical Devices (MeDe Innovation, Grant Number EP/K029592/1).

Open Access This article is distributed under the terms of the Creative Commons Attribution 4.0 International License (<http://creativecommons.org/licenses/by/4.0/>), which permits unrestricted use, distribution, and reproduction in any medium, provided you give appropriate credit to the original author(s) and the source, provide a link to the Creative Commons license, and indicate if changes were made.

References

- [1] Jin H-J, Park J, Karageorgiou V et al (2005) Water-stable silk films with reduced β -sheet content. *Adv Funct Mater* 15:1241–1247
- [2] Lu Q, Zhang B, Li M et al (2011) Degradation mechanism and control of silk fibroin. *Biomacromolecules* 12:1080–1086
- [3] Kataoka K, Scholz C, Vepari C, Kaplan DL (2007) Silk as a biomaterial. *Prog Polym Sci* 32:991–1007
- [4] Numata K, Subramanian B, Currie HA, Kaplan DL (2009) Bioengineered silk protein-based gene delivery systems. *Biomaterials* 30:5775–5784. doi:10.1016/j.biomaterials.2009.06.028
- [5] Omenetto FG, Kaplan DL (2010) New opportunities for an ancient material. *Science* 329:528–531
- [6] Hashimdeen SH, Miodownik M, Edirisinghe MJ (2013) Print head design and control for electrohydrodynamic printing of silk fibroin. *Mater Sci Eng C* 33(6):3309–3318
- [7] Zhang J-G, Mo X-M (2013) Current research on electrospinning of silk fibroin and its blends with natural and synthetic biodegradable polymers. *Front Mater Sci* 7(2):129–142
- [8] Valluzzi R, He SJ, Gido SP, Kaplan D (1999) Bombyx mori silk fibroin liquid crystallinity and crystallization at aqueous fibroin–organic solvent interfaces. *Int J Biol Macromol* 24:227–236. doi:10.1016/S0141-8130(99)00005-7

- [9] Huemmerich D, Slotta U, Scheibel T (2005) Processing and modification of films made from recombinant spider silk proteins. *Appl Phys A* 82:219–222. doi:[10.1007/s00339-005-3428-5](https://doi.org/10.1007/s00339-005-3428-5)
- [10] Li M, Ogiso M, Minoura N (2003) Enzymatic degradation behavior of porous silk fibroin sheets. *Biomaterials* 24:357–365
- [11] Tekin E, Smith PJ, Schubert US (2008) Inkjet printing as a deposition and patterning tool for polymers and inorganic particles. *Soft Matter* 4:703
- [12] Vilardell M, Granados X, Ricart S et al (2013) Flexible manufacturing of functional ceramic coatings by inkjet printing. *Thin Solid Films* 548:489–497
- [13] Zhang Y, Tse C, Rouholamin D, Smith PJ (2012) Scaffolds for tissue engineering produced by inkjet printing. *Cent Eur J Eng* 2:325–335
- [14] Delaney JT, Smith PJ, Schubert US (2009) Inkjet printing of proteins. *Soft Matter* 5:4866
- [15] Smith PJ, Morrin A (2012) Reactive inkjet printing. *J Mater Chem* 22:10965
- [16] Suntivich R, Drachuk I, Calabrese R et al (2014) Inkjet printing of silk nest arrays for cell Hosting. *Biomacromolecules* 15:1428–1435
- [17] Tao H, Marelli B, Yang M et al (2015) Inkjet printing of regenerated silk fibroin: from printable forms to printable functions. *Adv Mater* 27:4273–4279. doi:[10.1002/adma.201501425](https://doi.org/10.1002/adma.201501425)
- [18] Yamada H, Nakao H, Takasu Y, Tsubouchi K (2001) Preparation of undegraded native molecular fibroin solution from silkworm cocoons. *Mater Sci Eng C* 14:41–46. doi:[10.1016/S0928-4931\(01\)00207-7](https://doi.org/10.1016/S0928-4931(01)00207-7)
- [19] van den Berg AMJ, Smith PJ, Perelaer J et al (2007) Inkjet printing of polyurethane colloidal suspensions. *Soft Matter* 3:238. doi:[10.1039/b610017a](https://doi.org/10.1039/b610017a)
- [20] Barth A (2007) Infrared spectroscopy of proteins. *Biochim Biophys Acta* 1767:1073–1101. doi:[10.1016/j.bbabbio.2007.06.004](https://doi.org/10.1016/j.bbabbio.2007.06.004)
- [21] Hu X, Kaplan D, Cebe P (2006) Determining beta-sheet crystallinity in fibrous proteins by thermal analysis and infrared spectroscopy. *Macromolecules* 39:6161–6170. doi:[10.1021/ma0610109](https://doi.org/10.1021/ma0610109)
- [22] Tien LW, Gil ES, Park S-H et al (2012) Patterned silk film scaffolds for aligned lamellar bone tissue engineering. *Macromol Biosci* 12:1671–1679. doi:[10.1002/mabi.201200193](https://doi.org/10.1002/mabi.201200193)